Non-Coil, Optimal Sources for Wireless Powering of Sub-Millimeter Implantable Devices

Sanghoek Kim[1], John S. Ho[2], and Ada S. Y. Poon[3, *]

Abstract—This paper presents non-coil sources to improve the wireless power transfer efficiency for implantable device used in various medical applications — cardiovascular devices, endoscope in the small intestine, and neurostimulator in the brain. For each application, a bound on the power transfer efficiency and the optimal source achieving such bound are analytically solved. The results reveal that depending on the depth of the implantable devices, power can be transferred to a sub-millimeter scaled receiver with the efficiency ranging from $-57\,\mathrm{dB}$ to $-33\,\mathrm{dB}$, which is up to 6.6 times higher than the performance of existing coil-based source systems. The technique introduced in this paper can be broadly applied to other medical applications.

1. INTRODUCTION

Wireless delivery of energy to implantable devices is highly desirable, since it removes the necessity to replace a battery inside the device, and enables miniaturization of the device. Conventionally, researchers have chosen sufficiently low operating frequencies ($< 10\,\mathrm{MHz}$) to minimize the dielectric loss in tissue [1]. At such low frequencies, the receiver is in the near-field region of the source, and the link between the source and the receiver is modeled as an inductive coupling link [2–4].

However, when the device is much smaller than its distance from the source, the coupling between the coils is weak. Inductive coupled coils in this weakly coupled regime are generally very inefficient [5]. Recently, it has been shown that by operating at GHz-range frequencies, much higher power transfer efficiency can be achieved for a mm-scaled receiver [6]. At several centimeters of distance between the source and the receiver, operation at such frequency corresponds to the midfield.

More recently, source structures that exploit the characteristics of the midfield to significantly improve the power transfer efficiency were analytically solved [7, 8]. For the layered medium configuration shown in Fig. 1, the *equivalence principle* in electromagnetic theory ensures that the optimal efficiency obtained in [8] bounds the efficiency attainable by any physical realization of the source. The maximum efficiency was shown to be a function of the dielectric property of the tissue, distance between the source and receiver (z_f), and orientation (θ) of the receiver coil. The optimal source with its efficiency close to the global bound was physically realized and measured in [9].

To evaluate the benefits of the theory in other fields, this work solves the maximum efficiency and the optimal source structure for power transfer to µm-scaled receive coil in three different medical applications — a cardiovascular device to sense and stimulate heart signals [10], a wireless endoscope in the small intestine [11], and a neurostimulator in the brain to record neural activity [12]. In these three applications, the computed maximum efficiency for a receive coil of radius $400\,\mu\mathrm{m}$ lies from $-33\,\mathrm{dB}$ to $-57\,\mathrm{dB}$, for separation between the source and receiver ranging from $1.4\,\mathrm{cm}$ to $9.1\,\mathrm{cm}$. These efficiencies demonstrate 1.8 times to 6.6 times higher efficiency than existing coil-based sources (Table 1). Reminiscent of Shannon's channel capacity in information theory, this theory predicts that there is

* Corresponding author: Ada S. Y. Poon (adapoon@stanford.edu).
[1] Kyung Hee University, South Korea. [2] National University of Singapore, Singapore. [3] Stanford University, USA.

Table 1. Improvement of the efficiency by the optimization over the coil-based sources.

θ	Heart ($z_f = 5\,\mathrm{cm}$)	Intestine ($z_f = 9.1\,\mathrm{cm}$)	Brain ($z_f = 1.4\,\mathrm{cm}$)
$0°$	6.6 times	6.5 times	1.8 times
$90°$	3.5 times	3.2 times	2.5 times

significant room for improvement in efficiency of existing power transfer systems, and facilitates the design of structures to approach this optimal bound.

In this paper, we will use boldface letters for vectors and boldface capital letters with a bar such as $\bar{\mathbf{G}}$ for matrices. For a complex number x, $\mathrm{Re}\,x$ and $\mathrm{Im}\,x$ denote the real and imaginary part of x respectively. For a vector $\mathbf{r}$, r denotes its magnitude and $\hat{\mathbf{r}}$ is a unit vector denoting its direction. $(\cdot)^*$ denotes the conjugate operation.

2. MODEL AND PROBLEM FORMULATION

2.1. Tissue, Source, and Receiver Model

We model the inhomogeneity of the tissue as a planar multi-layered medium, as illustrated in Fig. 1. The tissue properties are modeled by assigning a dielectric permittivity ϵ to each layer. The dependence of ϵ with frequency is obtained from the Debye relaxation model [6].

Over the planar structure, we look for a source that maximizes the power transfer efficiency. It is difficult, however, to optimize it, since the shape of the source can be arbitrary in three dimensional space. The problem can be simplified by invoking the *equivalence principle* [13]. According to the equivalence principle, any arbitrary source can be represented by an equivalent surface (tangential) current density, $\mathbf{J}_1$, along a plane S_{src} between the source and medium as shown in Fig. 1. For the sake of convenience, S_{src} is assumed to be placed at $z = 0$.

As a result, without loss of generality, we model the source with surface electric current $\mathbf{J}_1$ on S_{src}
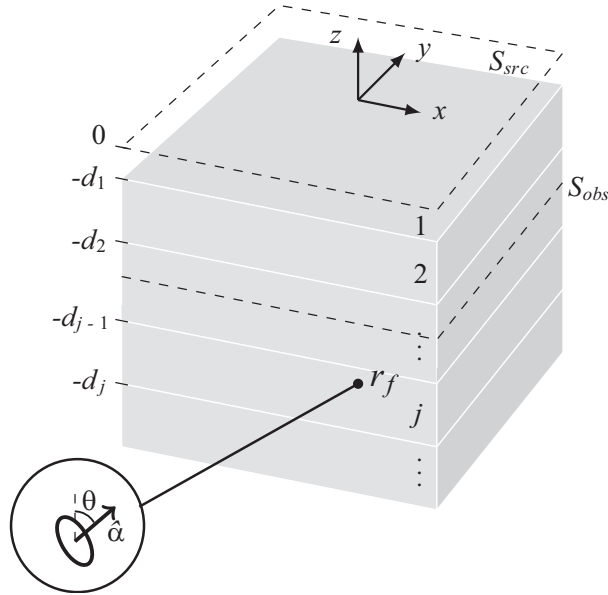

Figure 1. The layered medium model for tissue consists of n stacked layers where each layer is assigned a dielectric permittivity ϵ_{rj}. The center of the source is positioned at the origin and the receiver is placed at $\mathbf{r}_f = (0, 0, -z_f)$ with the norm of $\hat{\boldsymbol{\alpha}}$ in the layers.

in the rest of the paper:

$$\mathbf{J}_1(\mathbf{r}) = J_{1x}(\mathbf{r}_s)\,\delta(z)\,\hat{\mathbf{x}} + J_{1y}(\mathbf{r}_s)\,\delta(z)\,\hat{\mathbf{y}} \tag{1}$$

where $\mathbf{r}_s = x\hat{\mathbf{x}} + y\hat{\mathbf{y}}$. Finally, the receiver of miniature devices is modeled as a magnetic dipole with arbitrary orientation $\hat{\boldsymbol{\alpha}}$ located at $\mathbf{r}_f = (0, 0, -z_f)$ (Fig. 1):

$$\mathbf{M}_2(\mathbf{r}) = i\omega\mu A_r I_2\,\delta(x, y, z + z_f)\,\hat{\boldsymbol{\alpha}} \tag{2}$$

where $A_r I_2$ is the magnetic moment of the dipole, and $\hat{\boldsymbol{\alpha}}$ denotes the orientation of the magnetic dipole, which is tilted by θ from the z-axis. For a given $\mathbf{r}_f$ and $\hat{\boldsymbol{\alpha}}$, we want to find $J_{1x}(\mathbf{r}_s)$ and $J_{1y}(\mathbf{r}_s)$ that optimizes the power transfer efficiency.

2.2. Coupling Parameter

With reference to Fig. 2, we abstract the coupling between the source structure and receive coil as a *two-port network*:

$$\begin{aligned} V_1 &= Z_{11}I_1 + Z_{12}I_2 \\ V_2 &= Z_{21}I_1 + Z_{22}I_2. \end{aligned}$$

Since the receive coil is small, the source structure and receive coil are *loosely coupled*. The power transfer efficiency is then given by [7]

$$\eta = \frac{P_r}{P_t} \approx \frac{|Z_{21}|^2}{4R_{11}R_{22}} \frac{4R_{22}R_L}{|Z_{22} + Z_L|^2}. \tag{3}$$

where P_r is the received power at the output, and P_t is the transmit power at the input of the two-port network. The efficiency in Eq. (3) is the product of two factors: the *coupling efficiency* η_c on the left and the *matching efficiency* η_m on the right. The coupling efficiency is the ratio of the power available at the receiver to the input power. The matching efficiency is the ratio of the power delivered to the load to the available power, and is independent of transmit antenna structure. Note that for an inductively coupled system, $Z_{21} = Z_{12} = i\omega M$, where M is mutual inductance. Moreover, if the Z_{22} and Z_L are conjugately matched, Eq. (3) reduces to the expression of optimum efficiency for loosely coupled link in [14].

In this paper, as we focus on optimizing the source structure for a given receive coil, it suffices to maximize the coupling efficiency. From η_c, we extract the *coupling parameter* γ

$$\gamma = \frac{|Z_{21}|^2}{R_{11}} \tag{4}$$

which is completely determined by the source. The optimal source is thus given by the current distribution $\mathbf{J}_1(\mathbf{r}_s)$ that maximizes γ.
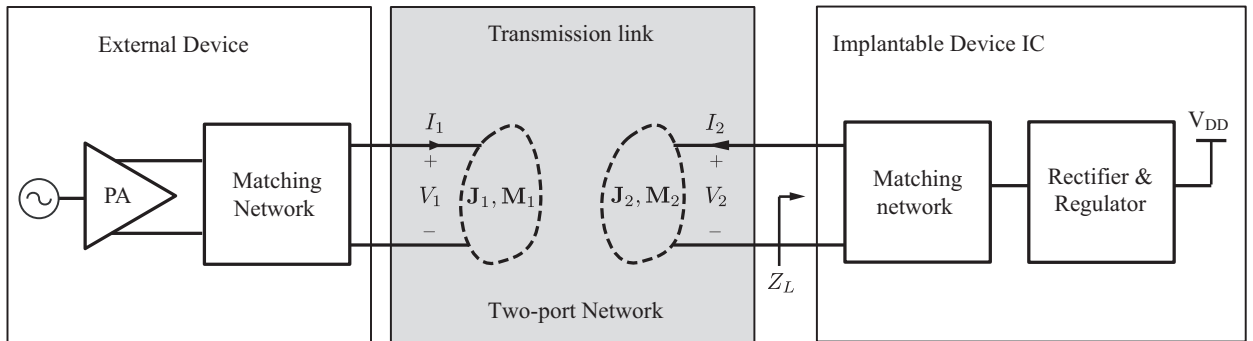

Figure 2. Flow of power in a wireless power transfer system.

3. THE OPTIMIZATION PROBLEM AND ITS SOLUTION

The derivation to find the current source $\mathbf{J}_1(\mathbf{r})$ that maximizes the efficiency was summarized in [8]. Here, we elaborate the detail of the derivation. To find the optimal source for a given receive coil, we will need to express the coupling parameter in terms of $\mathbf{J}_1$ first. This is achieved by first defining the impedances of the two-port network in terms of the electromagnetic fields from the sources $\mathbf{J}_1$. Then, we will derive these fields in terms of the source distributions, and find the source that maximizes the coupling parameter for the receive coil.

3.1. Self and Mutual Impedances

Under the assumption that the tissue loss dominates the total losses in the system, the coupling parameter can be expressed as

$$\gamma = \frac{|Z_{21}I_1|^2}{R_{11}|I_1|^2} = \frac{|V_{oc}|^2}{P_t} = \frac{\left|i\omega\mu A_r\,\boldsymbol{\alpha}\cdot\mathbf{H}_1(\mathbf{r}_f)\right|^2}{\omega\int_{z<-d_1}\operatorname{Im}\epsilon(\mathbf{r})\left|\mathbf{E}_1(\mathbf{r})\right|^2 d\mathbf{r}}, \tag{5}$$

where V_{oc} is the open-circuited voltage induced at the receive coil. The electromagnetic fields can be expressed in terms of Green's functions:

$$\mathbf{E}_1(\mathbf{r}) = i\omega\mu\int\bar{\mathbf{G}}_{ej}(\mathbf{r}-\mathbf{r}')\mathbf{J}_1(\mathbf{r}')\,d\mathbf{r}' \tag{6a}$$

$$\mathbf{H}_1(\mathbf{r}) = \int\bar{\mathbf{G}}_{hj}(\mathbf{r}-\mathbf{r}')\mathbf{J}_1(\mathbf{r}')\,d\mathbf{r}'. \tag{6b}$$

and taking the 2D Fourier transform with respect to (x,y) for a given z yields

$$\boldsymbol{\mathcal{E}}_1(\mathbf{k}_s,z) = i\omega\mu\bar{\boldsymbol{\mathcal{G}}}_{ej}(\mathbf{k}_s,z)\boldsymbol{\mathcal{J}}_1(\mathbf{k}_s) \tag{7a}$$

$$\boldsymbol{\mathcal{H}}_1(\mathbf{k}_s,z) = \bar{\boldsymbol{\mathcal{G}}}_{hj}(\mathbf{k}_s,z)\boldsymbol{\mathcal{J}}_1(\mathbf{k}_s). \tag{7b}$$

where $\mathbf{k}_s = k_x\hat{\mathbf{k}}_x + k_y\hat{\mathbf{k}}_y$. In multi-layered medium, the Green's functions for the nth layer are derived and presented in Appendix.

3.2. Upper-Bound on Efficiency

Now we express the coupling parameter in (5) in terms of $\boldsymbol{\mathcal{J}}_1(k_x,k_y)$. By the Parseval's theorem, for a Fourier transform pair $g(\mathbf{r}_s)$ and $G(\mathbf{k}_s)$, $\int|g(\mathbf{r}_s)|^2\,d\mathbf{r}_s = \frac{1}{4\pi^2}\int|G(\mathbf{k}_s)|^2\,d\mathbf{k}_s$, where $d\mathbf{k}_s = dk_x dk_y$. Therefore,

$$P_t = \frac{\omega}{4\pi^2}\iiint_{-\infty}^{-d_1}\operatorname{Im}\epsilon(z)\left|\boldsymbol{\mathcal{E}}_1(\mathbf{k}_s,z)\right|^2 dz\,d\mathbf{k}_s \tag{8}$$

$$= \iint\boldsymbol{\mathcal{J}}_1^*(\mathbf{k}_s)\bar{\mathbf{F}}(\mathbf{k}_s)\boldsymbol{\mathcal{J}}_1(\mathbf{k}_s)\,d\mathbf{k}_s,$$

where

$$\bar{\mathbf{F}}(\mathbf{k}_s) = \frac{\omega}{4\pi^2}\left(\int_{-\infty}^{-d_1}\operatorname{Im}\epsilon(z)\bar{\boldsymbol{\mathcal{G}}}_{ej}^*(\mathbf{k}_s,z)\bar{\boldsymbol{\mathcal{G}}}_{ej}(\mathbf{k}_s,z)\,dz\right).$$

As $\bar{\mathbf{F}}(\mathbf{k}_s)$ is Hermitian and positive semidefinite, it can be factored into [15]

$$\bar{\mathbf{F}}(\mathbf{k}_s) = \bar{\mathbf{U}}(\mathbf{k}_s)\bar{\boldsymbol{\Lambda}}(\mathbf{k}_s)\bar{\mathbf{U}}^*(\mathbf{k}_s),$$

where $\bar{\mathbf{U}}(\mathbf{k}_s)$ consists of orthonormal vectors. Vectors in $\bar{\mathbf{U}}(\mathbf{k}_s)$ have corresponding positive real eigenvalues in a diagonal matrix $\bar{\boldsymbol{\Lambda}}(\mathbf{k}_s)$. Defining $\boldsymbol{\mathcal{J}}_1'(\mathbf{k}_s) = \bar{\boldsymbol{\Lambda}}^{\frac{1}{2}}(\mathbf{k}_s)\bar{\mathbf{U}}^*(\mathbf{k}_s)\boldsymbol{\mathcal{J}}_1(\mathbf{k}_s)$ yields

$$P_t = \iint|\boldsymbol{\mathcal{J}}_1'(\mathbf{k}_s)|^2\,d\mathbf{k}_s.$$

For the numerator in Eq. (5) with $\mathbf{r}_f = (0, 0, -z_f)$, we have

$$\mathbf{H}_1(\mathbf{r}_f) = \frac{1}{4\pi^2} \iint \boldsymbol{\mathcal{H}}_1(\mathbf{k}_s, -z_f) \, d\mathbf{k}_s, \tag{9}$$

$$= \frac{1}{4\pi^2} \iint \bar{\boldsymbol{\mathcal{G}}}_{hj}(\mathbf{k}_s, -z_f) \boldsymbol{\mathcal{J}}_1(\mathbf{k}_s) \, d\mathbf{k}_s. \tag{10}$$

Defining

$$\mathbf{h}(\mathbf{k}_s) = \frac{1}{4\pi^2} \times \left[-i\omega\mu A_r \bar{\boldsymbol{\mathcal{G}}}_{hj}^*(\mathbf{k}_s, -z_f) \boldsymbol{\alpha} \right],$$

the coupling parameter in Eq. (5) can be written as

$$\gamma = \frac{|\iint \mathbf{h}^*(\mathbf{k}_s) \boldsymbol{\mathcal{J}}_1(\mathbf{k}_s) \, d\mathbf{k}_s|^2}{\iint |\boldsymbol{\mathcal{J}}_1'(\mathbf{k}_s)|^2 \, d\mathbf{k}_s} \tag{11}$$

$$= \frac{|\iint \mathbf{h}^*(\mathbf{k}_s) \bar{\mathbf{U}}(\mathbf{k}_s) \bar{\boldsymbol{\Lambda}}^{-\frac{1}{2}}(\mathbf{k}_s) \boldsymbol{\mathcal{J}}_1'(\mathbf{k}_s) \, d\mathbf{k}_s|^2}{\iint |\boldsymbol{\mathcal{J}}_1'(\mathbf{k}_s)|^2 \, d\mathbf{k}_s}$$

The optimization problem is to find $\boldsymbol{\mathcal{J}}_1(\mathbf{k}_s)$ such that the expression in (11) is maximized. By the Cauchy-Schwarz inequality, Eq. (11) is maximized when

$$\boldsymbol{\mathcal{J}}_{1,opt}'(\mathbf{k}_s) = \bar{\boldsymbol{\Lambda}}^{-\frac{1}{2}}(\mathbf{k}_s) \bar{\mathbf{U}}^*(\mathbf{k}_s) \mathbf{h}(\mathbf{k}_s) \tag{12}$$

or

$$\boldsymbol{\mathcal{J}}_{1,opt}(\mathbf{k}_s) = \bar{\mathbf{U}}(\mathbf{k}_s) \bar{\boldsymbol{\Lambda}}^{-1}(\mathbf{k}_s) \bar{\mathbf{U}}^*(\mathbf{k}_s) \mathbf{h}(\mathbf{k}_s), \tag{13}$$

and the optimal coupling parameter in (5) is

$$\gamma_{opt} = \iint |\bar{\boldsymbol{\Lambda}}^{-\frac{1}{2}}(\mathbf{k}_s) \bar{\mathbf{U}}^*(\mathbf{k}_s) \mathbf{h}(\mathbf{k}_s)|^2 \, d\mathbf{k}_s. \tag{14}$$

4. MATCHING EFFICIENCY

Optimizing the source yields the maximum coupling parameter γ_{opt}. The maximum coupling efficiency for a given receive coil is then given by

$$\eta_{c,opt} = \frac{\gamma_{opt}}{4R_{22}}. \tag{15}$$

The power transfer efficiency is given by the product of the coupling efficiency η_c and the matching efficiency η_m. The matching efficiency can be maximized subject to practical limitations that arises in the integrated circuits (IC) implementation [16, 17], and this paper briefly reviews the way introduced in [7] to calculate the maximum η_m.

The matching efficiency is given by

$$\eta_m = \frac{4R_{22}R_L}{|Z_{22} + Z_L|^2}, \tag{16}$$

where Z_{22} is the self-impedance of the coil receiver, and Z_L is the load impedance. Since the maximum matching efficiency $\eta_m = 1$ is achieved with the *conjugate matching* condition ($Z_L = Z_{22}^*$), we introduce a *matching network* between the receive coil and the load (rectifier) to control Z_L as shown in Fig. 2. However, practical limitations to conjugate matching arise from the limited transformation range of the matching network. For typical implants with load impedance on the order of $1 \, \mathrm{k\Omega}$ [16, 17], a limited Q-factor of matching network on the IC imposes the minimum load resistance condition

$$R_L > 10 \, \Omega. \tag{17}$$

When the self-resistance of coil receiver is small, this condition limits our ability to perform conjugate matching, and was taken into account to calculate the *achievable matching efficiency* $\eta_{m,av}$ for a given receiver. Finally, the maximum power transfer efficiency is the product of the maximum coupling efficiency and the achievable matching efficiency:

$$\eta_{opt} = \eta_{c,opt} \cdot \eta_{m,av}. \tag{18}$$

5. NUMERICAL EXAMPLES

So far, we have analytically derived the maximum power transfer efficiency η_{opt} for a multi-layered medium. In this section, we numerically evaluate the power transfer efficiency for small receive coil of radius $400\,\mu m$ in three different medical applications and compare the results with the efficiency of conventional coil sources.

5.1. Cardiovascular Devices

The source is placed $d_1 = 1\,cm$ above the air-skin interface while the receive coil is placed at 4 cm deep in the tissue ($z_f = 5\,cm$). The composition of the multi-layered model is summarized in Table 2. For simplicity, the last layer, heart, was modeled to extend to infinity.

Figure 3(a) shows the optimal coupling parameter γ_{opt} versus frequency when the implant is oriented in longitudinal direction ($\theta = 0°$, $\hat{\alpha} = \hat{z}$). For the purpose of comparison, the coupling parameters of coil sources with different diameters are shown. The coupling parameters of the coil sources were computed
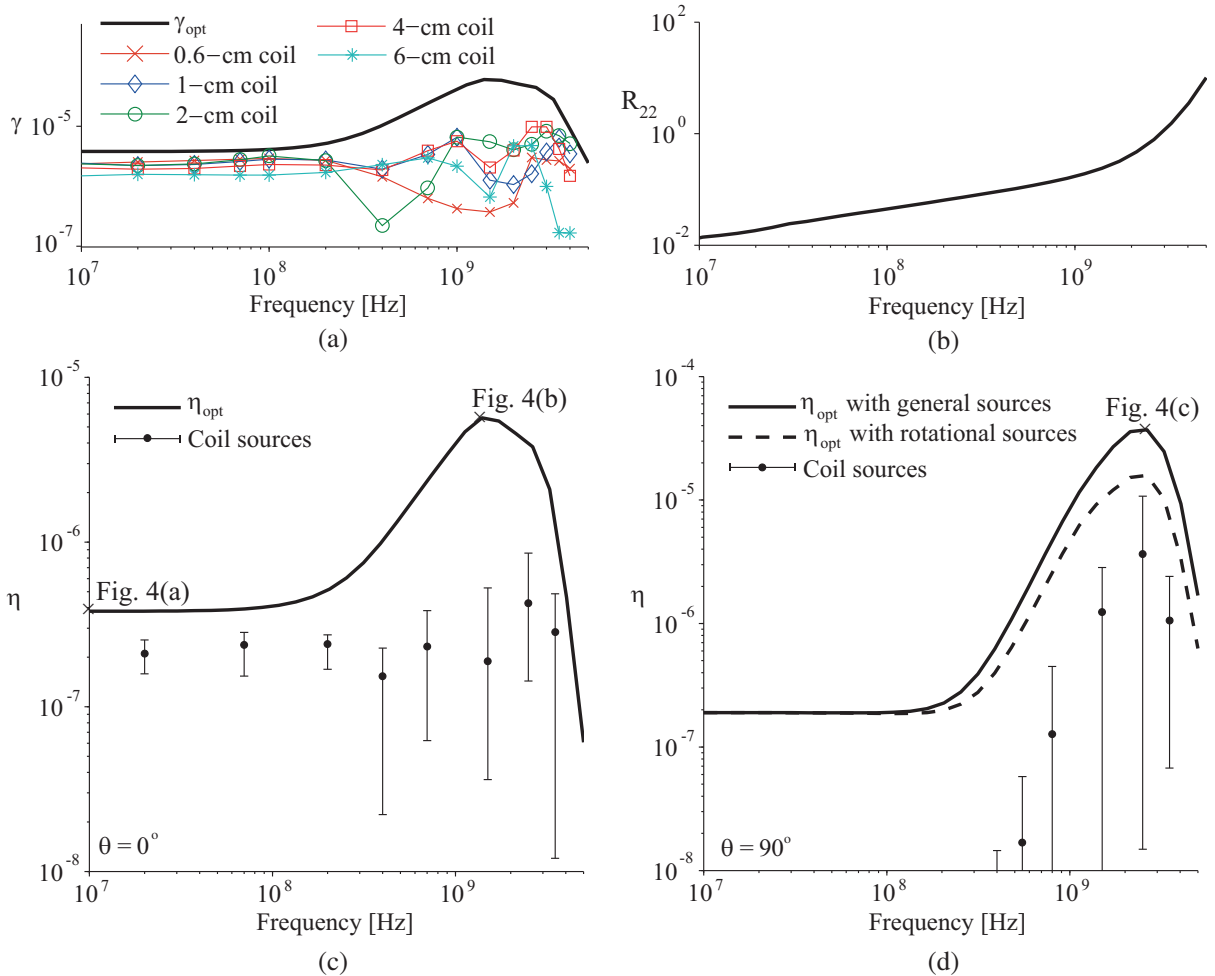

Figure 3. (a) Coupling parameter γ, (b) receiver self-resistance R_{22}, and (c) efficiency η as a function of frequency for a coil receiver with radius $400\,\mu m$ and $\theta = 0°$ in cardiovascular devices, (d) efficiency for a coil receiver with radius $400\,\mu m$ and $\theta = 0°$ in cardiovascular devices. Coil-based source structure with diameter from 0.6 to 6 cm (error bars show the max, min, and mean) achieve the efficiency well below the theoretical bound. The efficiency of coil-based sources are computed from a commercial EM simulator. The optimal source at denoted points are shown in Fig. 4.

Table 2. Tissue composition for several medical applications. Unit for the thickness (Δd) is millimeter.

	Layer 2		Layer 3		Layer 4		Layer 5		Layer 6	
	tissue	Δd	tissue	Δd	tissue	Δd	tissue	Δd	tissue	Δd
Heart	skin	2	fat	10	muscle	8	bone	16	heart	∞
Small intestine	skin	2	fat	24	muscle	20	colon	20	intestine	∞
Brain	skin	2	fat	2	bone	7	brain	∞	-	-

from an electromagnetic simulation tool, Mentor Graphics IE3D [18]. The diameters of coil sources were varied from 0.6 cm to 6 cm in the simulations. As in [6] and [7], we obtained the Z-parameters of links from the simulations and calculated γ of coil sources by (4). Fig. 3(b) presents the receiver R_{22} for a coil of area A_r surrounded by heart tissue and Fig. 3(c) shows the resulting power transfer efficiency η by Eq. (3).

At several centimeters of separation between the source and receive coil, frequencies less than 500 MHz correspond to the near field. The performance of the coils is within 20% of the bound in this region because the optimal source resembles a coil (Fig. 4(a)). The theoretical η_{opt}, however, exceeds the efficiency of coil sources by about 8.2 dB at higher frequency which corresponds to the midfield region. This improvement origins from intricate optimal source exploiting the characteristics of midfield. For example, at 1.4 GHz where the η_{opt} is peaked, the optimal source $\mathbf{J}_{1,opt}(\mathbf{r}_s)$ is shown in Fig. 4(b). The complicated rotational source, resembling a couple of coaxial coils with different radii and phases, brings about constructive interference at the implant location and destructive interference elsewhere to improve the efficiency. It is worthy to note that since a vertical magnetic dipole precisely generates rotational
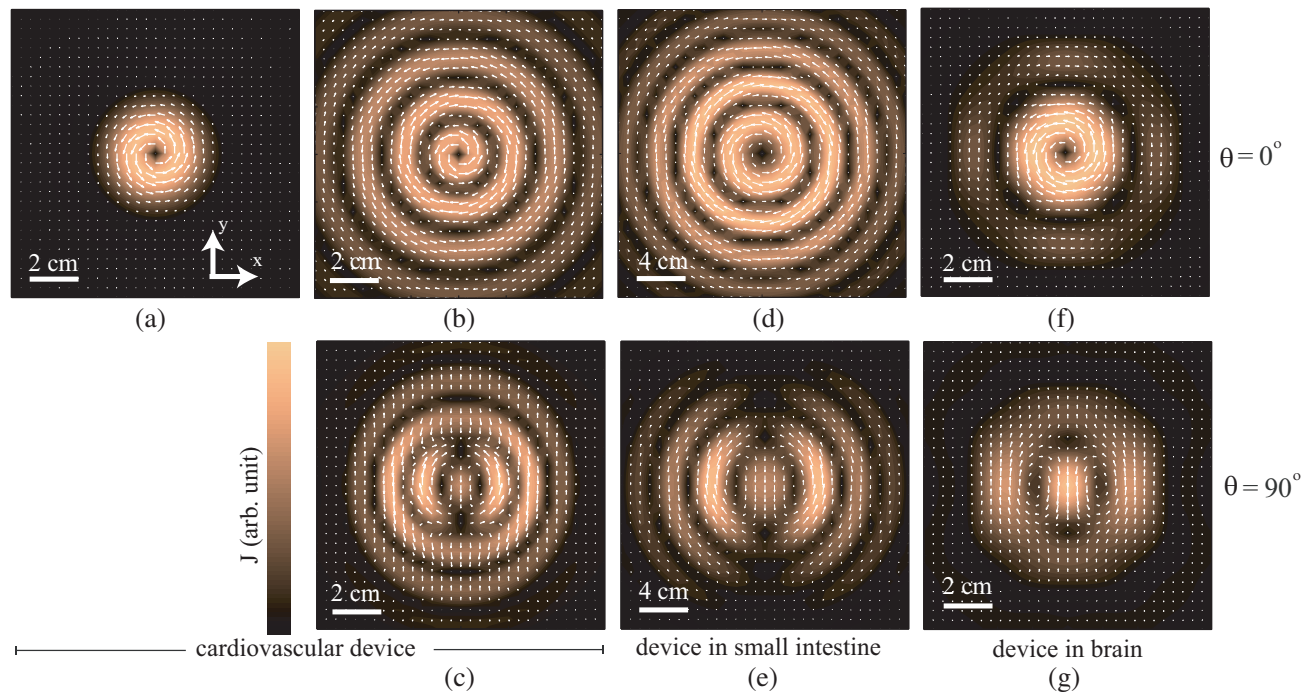

Figure 4. Optimal electric current density. For a cardiovascular devices with (a) $\theta = 0°$ at 10 MHz, (b) $\theta = 0°$ at 1.4 GHz, (c) $\theta = 90°$ at 2.6 GHz. For a device in small intestine with (d) $\theta = 0°$ at 910 MHz, (e) $\theta = 90°$ at 1.7 GHz. For a device in brain with (d) $\theta = 0°$ at 2.1 GHz, (e) $\theta = 90°$ at 3.3 GHz. For all the above plots, movies showing the current flow according to time are uploaded as supplementals online.

electric current, η_{opt} of (18) coincides with the η_{opt} obtained with optimal source of vertical magnetic current density in [7]. Beyond a low GHz-range, the advantage of midfield wanes because the dielectric loss of tissue increases significantly. This results in the optimal frequency residing in the low GHz-range.

We can compute theoretical η_{opt} for other orientation of the coil receiver as well. When the coil receiver is oriented in transverse direction ($\theta = 90°$, $\hat{\alpha} = \hat{x}$), Fig. 3(d) shows the theoretical η_{opt} and η of coil-based sources. Note that the η_{opt} again bounds the efficiency of coil-based sources for all the frequency range. Unlike the case for the receive coil in the longitudinal direction, the optimal source for the receive coil in the transverse direction requires both rotational and irrotational electric current. For example, the optimal source at 2.6 GHz where the η_{opt} is peaked, is shown in Fig. 4(c). Compared to the optimal source which consists of only vertical magnetic current density (dashed line in Fig. 3(d)), the component of irrotational electric current can further enhance the efficiency.

Finally, the efficiencies for different orientations of the receive coil are summarized in Fig. 5(a). Taking into account the tissue loss and practical constraints in receiver IC implementation, we can expect the power transfer efficiency for a coil receiver of diameter 400 µm in cardiovascular devices to be up to -43 dB, when operating at 2.6 GHz.
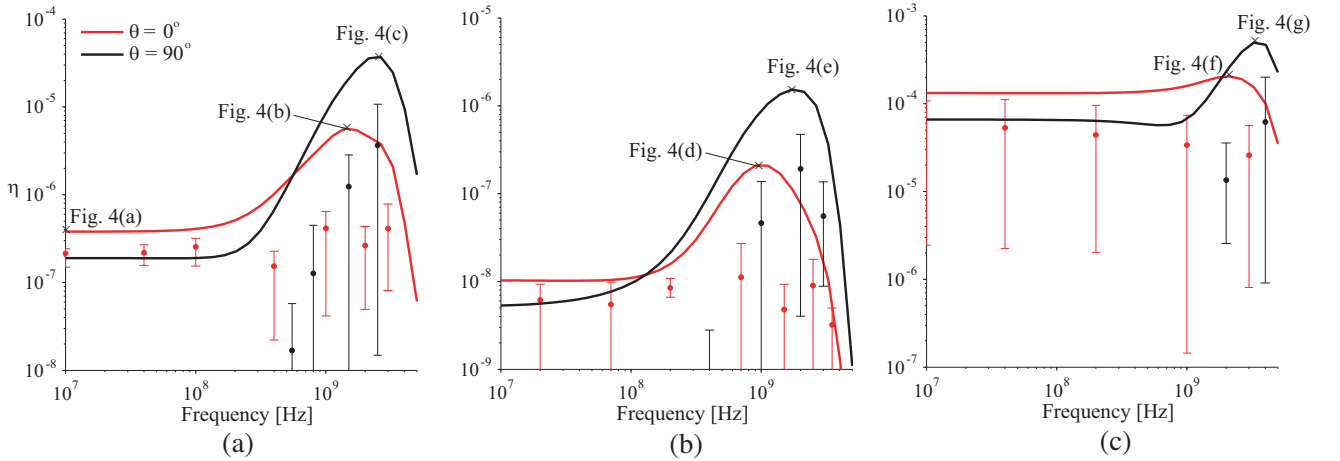

Figure 5. Efficiency η as a function of frequency for a receive coil of radius 400 µm in (a) heart, (b) small intestine, and (c) brain. Coil-based source structure with diameter from 0.6 to 6 cm (error bars show the max, min, and mean) achieve the efficiency well below the theoretical bound. The efficiency of coil-based sources are computed from a commercial EM simulator.

5.2. Devices in Small Intestine

Similarly, theoretical η_{opt} can be obtained for devices in the small intestine. Again, the tissue composition is summarized in Table 2. The devices is at $z_f = 9.1$ cm with $d_1 = 1$ cm. Theoretical η_{opt} and η of coil-based sources versus frequency are shown in Fig. 5(b).

The optimization and simulation results are generally similar to those from the cardiovascular devices. When the receive coil is along the longitudinal direction and is placed in the near field, the optimal source resembles a coil. The efficiency of a coil source is close to the optimal efficiency. At higher frequency corresponding to the midfield, the efficiency for a receive coil in the transverse direction outperforms the receive coil in the longitudinal direction, because the radiative field becomes more significant than the reactive field.

Since the receive coil in the small intestine is placed deeper in tissue than that in the heart, the efficiency is obviously worse than that of the cardiovascular devices. By operating at 1.7 GHz, power transfer efficiency for a 400-µm radius receive coil in small intestine can reach up to -57 dB. Also, since the separation between the source and receive coil is longer, the dimension of the optimal source is larger as shown in Figs. 4(d) and (e).

5.3. Devices in Brain

As a last numerical example, we model the tissue compositions for devices in the brain as summarized in Table 2. Here, the receive coil is at $z_f = 1.4\,\text{cm}$ with $d_1 = 2\,\text{mm}$. Fig. 5(c) shows the theoretical η_{opt} and efficiencies of coil sources for the receive coil with $\theta = 0°$. Since the separation between the source and receive coil is much shorter, Fig. 4(f) shows that the optimal source is similar to a coil even at 2.1 GHz where the η_{opt} is peaked. The improvement by optimization is only 2.6 dB. When the receive coil is in the transverse direction, the optimal source shown in Fig. 4(g) achieves $-33\,\text{dB}$ at 3.3 GHz, outperforming the best coil-based design by 3.9 dB.

In summary, the ratio of peaks between theoretical η_{opt} and the efficiency of coil sources for various medical applications are tabulated in Table 1. When the receive coil is shallowly embedded, the improvement on the efficiency by optimization is not significant. However, when the receive coil is deeply embedded, the improvement by optimization over conventionally coil-based sources ranges from 5 to 8 dB for a receive coil of radius 400 µm.

6. CONCLUSION

We studied the upper-bound on the power transfer efficiency for a small receiver embedded in multiple planar layers of tissue. For various medical applications, the maximum efficiency was solved and compared with those of conventional coil sources.

We verified that the optimal efficiency indeed bounds the efficiency of coil sources from simulation. Moreover, the comparison reveals that we have significant room for improvement in efficiency over existing power transfer systems. The improvement tends to increase with the source-receive separation, reaching 8 dB of improvement when the receiver is deeply embedded. Such remarkable improvement takes place because of complicated optimal source exploiting the characteristics of the midfield. An example of physical realization of the optimal source was demonstrated in [8].

APPENDIX A. DERIVATION OF GREEN'S FUNCTIONS

In free-space, via the use of Weyl identity, the Green's functions in spectral domain are given by

$$\bar{\boldsymbol{\mathcal{G}}}_{ej,fs}(k_x, k_y, z) = \bar{\boldsymbol{\mathcal{G}}}_{hm,fs}(k_x, k_y, z) = \frac{ie^{-ik_z z}}{2k_z}\left(\bar{\mathbf{I}} - \frac{\mathbf{k}\mathbf{k}^t}{k^2}\right)$$

$$\bar{\boldsymbol{\mathcal{G}}}_{hj,fs}(k_x, k_y, z) = \bar{\boldsymbol{\mathcal{G}}}_{em,fs}(k_x, k_y, z) = -\frac{e^{-ik_z z}}{2k_z}\mathbf{k} \times \bar{\mathbf{I}},$$

where $k_z = \sqrt{k^2 - k_x^2 - k_y^2}$, k is the wavenumber of free-space, and $\mathbf{k} = [k_x\ k_y\ -k_z]^t$. In general, the reflection and transmission coefficients in TM waves differ from those in TE waves. Therefore, to solve the fields in multi-layered medium, the waves are first decomposed into TM and TE components, and corresponding reflection and the transmission coefficients should be incorporated [19, Chapter 2]. The E_z and H_z should be solved first since they characterize TM waves and TE waves, respectively. For example, when z is in between $-d_{n+1}$ and $-d_n$, the z-component of Green's functions for electric field can be written as

$$\hat{\mathbf{z}}^t\bar{\boldsymbol{\mathcal{G}}}_{ej,n}(k_x, k_y, z) = \frac{i}{2k_{1z}} \times \hat{\mathbf{z}}^t\left(\bar{\mathbf{I}} - \frac{\mathbf{k}_1\mathbf{k}_1^t}{k_n^2}\right) A_n^{TM}\left[e^{-ik_{nz}z} + \tilde{R}_{n,n+1}^{TM}e^{ik_{nz}(z+2d_n)}\right]$$

$$\hat{\mathbf{z}}^t\bar{\boldsymbol{\mathcal{G}}}_{em,n}(k_x, k_y, z) = -\frac{1}{2k_{1z}} \times \hat{\mathbf{z}}^t\left(\mathbf{k}_1 \times \bar{\mathbf{I}}\right) A_n^{TM}\left[e^{-ik_{nz}z} + \tilde{R}_{n,n+1}^{TM}e^{ik_{nz}(z+2d_n)}\right]$$

where $k_{nz} = \sqrt{k_n^2 - k_x^2 - k_y^2}$ and k_n is the wavenumber of the nth layer, and $\mathbf{k}_1 = [k_x\ k_y\ -k_{1z}]^t$. $\tilde{R}_{n,n+1}^{TM/TE}$ is the generalized reflection coefficients and $A_n^{TM/TE}$ can be interpreted as the generalized transmission cofficient. Their expressions can be found in [19, Chapter 2]. Given the Green's functions of the $\hat{\mathbf{z}}$-components of the electromagnetic field, the Green's function of the transverse components can also be derived in each of the homogeneous layers.

REFERENCES

1. RamRakhyani, A., S. Mirabbasi, and M. Chiao, "Design and optimization of resonance-based efficient wireless power delivery systems for biomedical implants," *IEEE Trans. Biomed. Circuits Syst.*, Vol. 5, 48–63, Feb. 2011.

2. Heetderks, W. J., "RF powering of millimeter- and submillimeter-sized neural prosthertic implants," *IEEE Trans. Biomed. Eng.*, Vol. 35, 323–327, May 1988.

3. Donaldson, N. N. and T. Perkins, "Analysis of resonant coupled coils in the design of radio frequency transcutaneous links," *Med. Biol. Eng. Comput.*, Vol. 21, 612–627, Sep. 1983.

4. Chen, C.-J., T.-H. Chu, C.-L. Lin, and J.-C. Jou, "A study of loosely coupled coils for wireless power transfer," *IEEE Trans. Circuits Syst. — II: Express Briefs*, Vol. 57, 536–540, Jul. 2010.

5. Ho, J. S., S. Kim, and A. S. Y. Poon, "Midfield wireless powering for implantable systems," *Proceedings of the IEEE*, Vol. 101, No. 6, 1369–1378, 2013.

6. Poon, A. S. Y., S. O'Driscoll, and T. H. Meng, "Optimal frequency for wireless power transmission into dispersive tissue," *IEEE Trans. Antennas And Propagation*, Vol. 58, 1739–1750, May 2010.

7. Kim, S., J. S. Ho, and A. S. Y. Poon, "Wireless power transfer to miniature implants: Transmitter optimization," *IEEE Trans. Antennas and Propagation*, Vol. 60, No. 10, 2012.

8. Kim, S., J. S. Ho, and A. S. Y. Poon, "Midfield wireless powering of subwavelength autonomous devices," *Physical Review Letters*, Vol. 110, 1–5, May 2013.

9. Ho, J. S., A. J. Yeh, E. Neofytou, S. Kim, Y. Tanabe, B. Patlolla, R. E. Beygui, and A. S. Y. Poon, "Wireless power transfer to deep-tissue microimplants," *Proceedings of the National Academy of Sciences*, Vol. 111, No. 22, 7974–7979, 2014.

10. EBR System Inc., "Implantable systems for wireless heart stimulation," www.ebrsystemsinc.com, 2011.

11. Lenaerts, B. and R. Puers, "An inductive power link for a wireless endoscope," *Biosnes. Bioelectron.*, Vol. 22, 1390–1395, 2007.

12. Biederman, W., D. J. Yeager, N. Narevsky, A. C. Koralek, J. M. Carmena, E. Alon, and J. M. Rabaey, "A fully-integrated, miniaturized ($0.125\,\mathrm{mm}^2$) $10.5\,\mu$w wireless neural sensor," *IEEE Journal of Solid-State Circuits*, Vol. 48, No. 4, 960–970, 2013.

13. Harrington, R. F., *Time-Harmonic Electromagnetic Fields*, IEEE Press, 2001.

14. Ko, W. H., S. P. Liang, and C. D. F. Fun, "Design of radio-frequency powered coils for implant instruments," *Med. Biol. Eng. Comput.*, Vol. 15, 634–640, Feb. 1977.

15. Strang, G., *Linear Algebra and Its Application*, 3rd Edition, Saunders College Publishing, 1988.

16. O'Driscoll, S., A. S. Y. Poon, and T. H. Meng, "A mm-sized implantable power receiver with adaptive link compensation," *Proc. IEEE Intl. Solid-State Circuits Conf. (ISSCC)*, Feb. 2009.

17. Yakovlev, A., D. Pivonka, T. H. Meng, and A. S. Y. Poon, "A mm-sized wirelessly powered and remotely controlled locomotive implantable device," *Proc. IEEE Intl. Solid-State Circuits Conf. (ISSCC)*, Feb. 2012.

18. We solve Maxwell's equations for all physical sources using the method-of-moments (Mentor Graphics, IE3D).

19. Chew, W. C., *Waves and Fields in Inhomogeneous Media*, IEEE Press, 1995.